THERMAL METHANOL OBSERVATIONS OF THE OUTFLOW FROM THE G31.41+0.31 HOT MOLECULAR CORE

E. Araya,[1,2] P. Hofner,[1,2] S. Kurtz,[3] L. Olmi,[4,5] AND H. Linz[6]

ABSTRACT

The G31.41+0.31 region hosts one of the most prominent hot molecular cores known. Coincident with the hot molecular core is an outflow whose orientation has been controversial. We report VLA-C observations of thermal methanol (7_0–6_1 A^+, 44 GHz) toward the position of the G31.41+0.31 hot molecular core. Our goals are to clarify the orientation of the outflow and to study the properties of a molecular outflow from a very young region of massive star formation. We confirm that the outflow is indeed associated with the hot molecular core. Our observations strongly suggest that the outflow is oriented in the northeast-southwest direction. The outflow is massive ($\gtrsim 15\,M_\odot$), with a dynamical time of the order of $\sim 4 \times 10^3$ yr, and has a wide-angle bipolar morphology.

Subject headings: H II regions — ISM: clouds — ISM: individual (G31.41+0.31) — ISM: molecules — radio lines: ISM

1. INTRODUCTION

Massive stars are of critical importance for a number of processes related to Galactic structure and evolution of the interstellar medium (ISM). Nevertheless, their formation and early evolution are poorly understood (e.g., Stahler et al. 2000). Widely disparate formation models have been proposed, including monolithic and competitive accretion; as well as coalescence (e.g., Yorke et al. 1995; Bonnell et al. 1998; Keto & Wood 2006; Bonnell & Bate 2006). As yet there is no consensus as to which mechanism is the most promising, although in recent years indirect evidence (e.g., outflows and jets) appears to favor the disk accretion scenario. One result that is more clearly established is that the massive star formation process occurs within hot molecular cores (HMCs; e.g., Kurtz et al. 2000 and references therein). HMCs host a wealth of star formation phenomena including outflows, masers, and possibly accretion disks (Cesaroni et al. 2005; see also Cesaroni et al. 2007). Whatever the ultimate answer to the nature of the massive star formation process, it is likely to be achieved by studies of HMCs, their structure, and the phenomena occurring within them.

G31.41+0.31 is a massive star formation site located at a distance of ~ 7.3 kpc (Sewiło et al. 2004). Cesaroni et al. (1998; see also Cesaroni et al. 1994a) conducted VLA observations of highly excited ammonia [NH_3 (4,4)] and their data reveal hot (>200 K), dense ($>10^7$ cm^{-3}) molecular gas within a region less than 0.1 pc in size, i.e., a HMC. Theoretical considerations suggest that such a core should be internally heated (Kaufman et al. 1998) and indeed, high angular resolution VLA continuum observations (Araya et al. 2003; P. Hofner et al., in preparation) show two 7 mm continuum sources at the center of the HMC

oriented in a northeast-southwest direction; at least one of them could be caused by free-free emission from a bow shock. In addition to NH_3, other molecular species show prominent emission in this region, for example CH_3CN (Cesaroni et al. 1994b; Olmi et al. 1996; Beltrán et al. 2004; Araya et al. 2005), H_2S (Gibb et al. 2004), and SiO and HCO^+ (Maxia et al. 2001). Olmi et al. (1996) conducted Plateau de Bure Interferometer (PdBI) ^{13}CO observations of the region and report a molecular outflow centered at the HMC position, and oriented in a northwest-southeast direction (i.e., almost perpendicular to the orientation of the 7 mm continuum sources). However, the interpretation of the ^{13}CO data is difficult given the relatively low angular resolution, the large extent of the ^{13}CO emission, sparse u-v sampling, and the presence of several ^{13}CO clumps in their map. The G31.41+0.31 region also shows prominent OH (Gaume & Mutel 1987), CH_3OH (Kurtz et al. 2004), and H_2O (Hofner & Churchwell 1996) maser emission (see § 5). In particular, the 22 GHz H_2O masers mapped by Hofner & Churchwell (1996) show a northeast-southwest distribution which is approximately parallel to the orientation of the two 7 mm sources in the HMC (Araya et al. 2003; P. Hofner et al. in preparation).

The outflow in the G31.41+0.31 region is particularly interesting because it is associated with the HMC. It is thought that HMCs precede ultracompact H II (UCH II) regions in the evolutionary sequence (e.g., Churchwell 2002), so it is likely that the G31.41+0.31 outflow is still quite young. The orientation of the molecular outflow in G31.41+0.31 is controversial. As mentioned above, Olmi et al. (1996) report that the outflow is oriented in a northwest-southeast direction, and this has been used by other authors (e.g., Beltrán et al. 2004) to argue that the northeast-southwest velocity gradient observed in several molecular lines (see § 5) is tracing a molecular torus (or disk) instead of a molecular outflow. Other authors (Gibb et al. 2004), report that the outflow is not in the northwest-southeast direction but in the east-west direction. Thus, with the objectives of clarifying the direction of the outflow in the G31.41+0.31 HMC, its relationship with the 7 mm continuum sources in the region, and its characteristics as an outflow from a very young region of massive star formation, we conducted high angular resolution CH_3OH 44 GHz observations with the VLA to image the thermal CH_3OH emission of the HMC.

[1] New Mexico Institute of Mining and Technology, Physics Department, 801 Leroy Place, Socorro, NM 87801.

[2] National Radio Astronomy Observatory, P.O. Box 0, Socorro, NM 87801.

[3] Centro de Radioastronomía y Astrofísica, Universidad Autónoma de México, Apdo. Postal 3-72, 58089, Morelia, Michoacán, Mexico.

[4] Istituto di Radioastronomia, INAF, Sezione di Firenze, Largo Enrico Fermi 5, I-50125 Florence, Italy.

[5] University of Puerto Rico at Rio Piedras, Physics Department, P.O. Box 23343, San Juan, PR 00931.

[6] Max-Planck-Institut für Astronomie, Königstuhl 17, D-69117 Heidelberg, Germany.

2. OBSERVATIONS

The observations were conducted on 2004 March 22, with the VLA in the C configuration.[7] We observed the methanol (CH$_3$OH) 7_0–6_1 A^+ (ν_0 = 44069.43 MHz, E_u = 64.9 K) transition using 1 IF mode, a bandwidth of 12.5 MHz ($\sim$85 km s^{-1}), 64 channels (195.3 kHz channel width, $\sim$1.3 km s^{-1}), and a central bandpass velocity of 98.2 km s^{-1}. The primary beam of the VLA antennas at this frequency is approximately 1'. The phase tracking center was R.A. = 18^{h}47^{m}34.60^s, decl. = $-01°12'46.0''$ (J2000.0). We observed the quasars 3C 286 (J1331+305), J1256$-$057, and J1851+005 as flux, bandpass, and phase calibrators, respectively. For the flux calibrator 3C 286 we assumed $S_{44\,GHz}$ = 1.43 Jy, and we measured flux densities of 12.3 and 0.76 Jy for the bandpass and phase calibrators, respectively. The observing mode was fast-switching with a cycle of 60/40 s (source/calibrator). The total time on source was approximately 1.5 hr.

The data reduction was conducted with AIPS following the standard procedure for VLA high-frequency observations. We obtained Hanning smoothed data cubes using natural (θ_{syn} = 0.63'' × 0.49'', P.A. = $-13°$, rms = 1.8 mJy b^{-1}) and uniform (θ_{syn} = 0.44'' × 0.41'', P.A. = $-23°$, rms = 2.8 mJy b^{-1}) weightings. Radio continuum emission at 7 mm was detected and removed from the data before imaging of the final CH$_3$OH data cubes. Instead of discussing our low-angular resolution and narrow bandwidth 7 mm detection, we use the higher signal-to-noise and higher spatial resolution 7 mm continuum observations by Araya et al. (2003; P. Hofner et al., in preparation); see Figures 1, 4, and 5.

3. RESULTS

As in the lower angular resolution observations of Kurtz et al. (2004), we detected thermal[8] and maser CH$_3$OH emission in the G31.41+0.31 region. In Figure 1 we show the zeroth- and first-moment velocity maps of the natural weighted data cube. We also show the 3.6 cm and 7 mm radio continuum from Araya et al. (2003; P. Hofner et al., in preparation) in the top and bottom panels, respectively. Thermal CH$_3$OH emission is detected toward the HMC position (see Figs. 1 and 2). A clear northeast-southwest velocity gradient is observed in the intensity-weighted velocity field (hereafter velocity map; Fig. 1, *bottom panel*). CH$_3$OH maser emission is distributed throughout the region. Given the large synthesized beam and low spectral resolution of our observations, we cannot unequivocally distinguish between a thermal or nonthermal origin for the CH$_3$OH emission that is not associated with the HMC. Nevertheless, we favor the nonthermal (maser) interpretation because of spatially unresolved emission and/or narrow line widths (e.g., Fig. 2). Taking maser 5 as reference position (Fig. 1, *bottom panel*), blueshifted masers are predominately located in the southwest of the map, whereas redshifted masers are mostly found in an east-northeast region. The masers appear to be primarily distributed toward the edges of the radio continuum emission, i.e., the boundary between ionized and molecular gas. A velocity gradient in the CH$_3$OH masers (blueshifted [northeast]–redshifted [southwest]) is detected along a line toward the circular (shell-like) UCH II region (masers 13 and 14; $\sim$4'' northeast from the HMC, see Fig. 1, *bottom panel*). The line parameters of the thermal and maser CH$_3$OH emission obtained from the natural weighted data cube

[8] In this paper we will use "thermal emission" meaning "quasi-thermal emission," because maser emission may be blended with the thermal component.
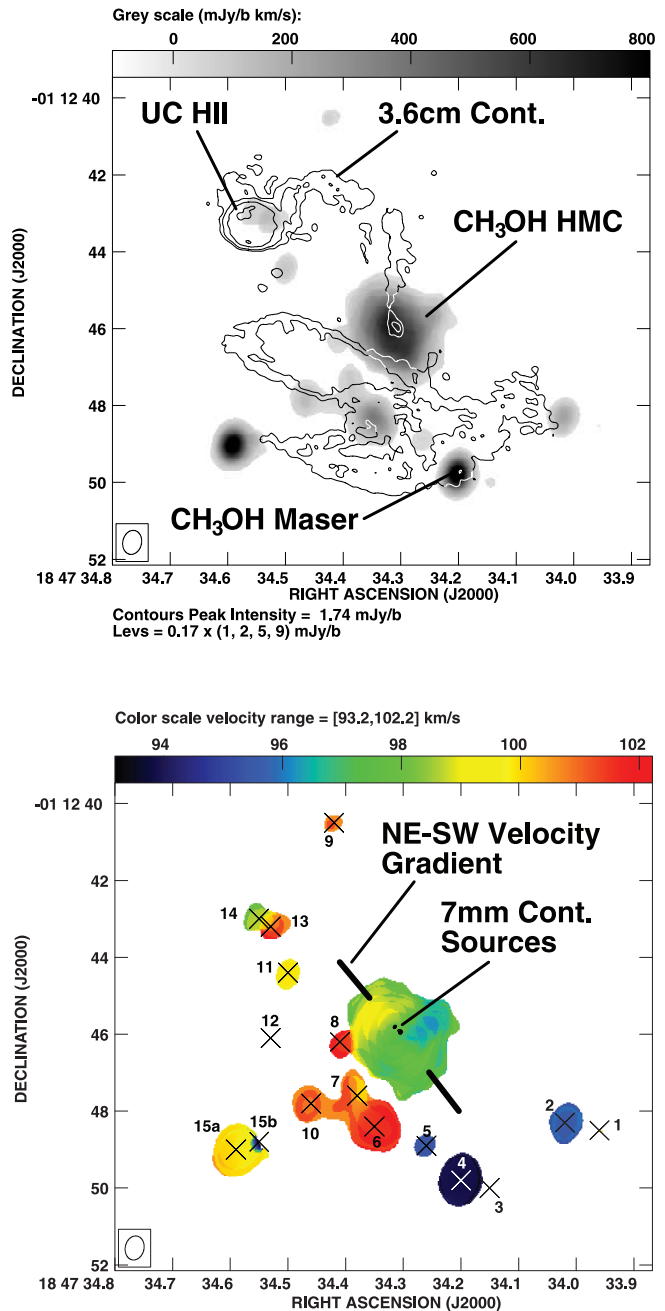
Fig. 1.— *Top*: We show the integrated intensity map obtained from the natural weighted CH$_3$OH data cube; the 3.6 cm radio continuum from Araya et al. (2003; P. Hofner et al., in preparation) is shown in contours. Note the extended CH$_3$OH emission detected toward the position of the HMC. The brightness temperature of the CH$_3$OH emission at the position of the HMC is $\sim$80 K, and thus the emission is likely thermal at that position. All other CH$_3$OH emission in the figure appears to be maser (for clarity, only one component was explicitly marked as maser; but all are marked with crosses in the bottom panel). However, we cannot rule out additional thermal emission not associated with the HMC given the low spectral and spatial resolution of our observations. *Bottom*: Intensity-weighted velocity field obtained from the natural weighted CH$_3$OH data cube is coded by colors. We also mark the position of the two 7 mm radio continuum sources reported by Araya et al. (2003; P. Hofner et al. in preparation), and the direction of the velocity gradient and core elongation as determined by visual inspection. The identification number of the masers is explicitly shown (see Table 1). To produce the figures, signal below 10σ in the CH$_3$OH data cube was clipped to improve contrast.

FIG. 2.—Examples of CH$_3$OH spectra obtained from the natural weighted data cube. The CH$_3$OH spectrum of the HMC (*top panel*) shows a broad (FWHM = 7.9 km s^{-1}) Gaussian line. An example of one of the masers profiles is shown in the bottom panel.

are reported in Table 1. The line widths of the maser lines listed in Table 1 are upper limits because of the relatively large channel width of the observations (1.3 km s^{-1}) and the use of Hanning smoothing.

In Figure 3 we show the position-velocity (PV) diagram along the northeast-southwest velocity gradient (i.e., the major axis of the HMC). The PV diagram shows two main velocity components at $\sim$98 km s^{-1} separated by $\sim$1″. The brightest component (southwest) is the peak of the thermal CH$_3$OH emission; however, it may have contributions from CH$_3$OH maser emission embedded in the HMC. Future higher angular resolution observations are required to establish whether the brightest component is partially due to maser emission. The PV diagram shows a non-Keplerian velocity distribution around the HMC center that has a linear velocity-distance component (a "Hubble-Law" velocity field) as observed in a number of outflows (e.g., Arce et al. 2007).

4. CH$_3$OH OUTFLOW IN G31.41+0.31

Based on our observations the diameter of the HMC is $\sim$0.14 pc (28×10^3 AU). Using only data from the inner 0.09 pc region of the core (to minimize contamination due to nearby masers), the FWHM of the CH$_3$OH thermal emission is $\sim$7.9 km s^{-1}; the correspondent mass of a virialized core of such characteristics is

greater than $\sim$700 $M_\odot$.[9] In order to estimate the total gas mass in the region (following Mehringer & Menten 1997), we assume optically thin CH$_3$OH emission and a CH$_3$OH abundance of 10^{-6}, i.e., similar to the abundance measured in the Orion star-forming region (Mehringer & Menten 1997 and references therein). We also assume a gas temperature of 180 K, i.e., the average of the core and halo temperatures based on CH$_3$CN observations by Olmi et al. (1996). The gas mass derived from our CH$_3$OH observations is $\sim$340 $M_\odot$, in agreement with the 350 $M_\odot$ value obtained from 3 mm dust continuum observations (Gibb et al. 2004 based on Maxia et al. 2001 data).[10] That the virial mass is greater than the gas mass suggests that the kinematic structure traced by the velocity gradient is not stable; this could be caused by an outflow or by an unstable molecular torus (e.g., Cesaroni et al. 1994b). We note that the gas mass value could match the virial mass if the CH$_3$OH abundance were a factor of $\sim$2 smaller than the assumed value.

To explore the nature of the northeast-southwest velocity gradient detected in the HMC (see Fig. 1, *bottom panel*), we created uniform weighted maps to increase the angular resolution. In Figure 4 we show the channel maps of the CH$_3$OH emission associated with the HMC obtained from the uniform weighted cube. We also mark the position of the 7 mm radio continuum sources from Araya et al. (2003; P. Hofner et al., in preparation). In Figure 5 we show a composite figure of the 92.9 and 103.5 km s^{-1} CH$_3$OH channel maps shown in Figure 4. The morphology observed in the 92.7 and 103.5 km s^{-1} channel maps is consistent with a wide angle molecular outflow oriented in the northeast-southwest direction. Although the physical properties of the G31.41+0.31 outflow clearly indicate an origin from a massive object (see below), it is interesting to point out the morphological similarity to outflows detected toward low-mass star-forming regions such as the CO (1–0) outflow in L1228 (Arce & Sargent 2004). The orientation of the outflow is parallel to the line connecting the two 7 mm radio continuum sources. Given that one or both of the continuum sources could be tracing ionized bow shocks (P. Hofner et al., in preparation), this parallel orientation further supports the outflow interpretation for the CH$_3$OH velocity gradient.

In the case of the outflow interpretation, assuming conical symmetry with an inclination angle of 45°, and following Mehringer & Menten (1997) and Gibb et al. (2004), we estimate the following outflow properties: a dynamical time of the order of $\sim$4 × 10^3 yr, mass in the outflow $\sim$15 $M_\odot$, kinetic energy $\sim$8 × 10^{45} ergs, a momentum of $\sim$110 $M_\odot$ km s^{-1}, a mass flow rate of $\sim$4 × 10^{-3} $M_\odot$ yr^{-1}, and a mechanical luminosity of $\sim$20 $L_\odot$. These estimates must be considered lower limits because we used only the properties of a single red and blue channel (Fig. 5) for the calculations, we assumed optically thin emission, the CH$_3$OH abundance could be smaller (the total mass is inversely proportional to the abundance; we assumed an abundance of 10^{-6}, see above), and our CH$_3$OH observations are not sensitive to gas at densities substantially lower than 10^7 cm^{-3}. These values are similar to those measured for other outflows from massive star-forming regions in the Galaxy (e.g., Wink et al. 1994; Shepherd et al. 1998; Klaassen et al. 2006), and thus our outflow interpretation of the CH$_3$OH velocity gradient is physically reasonable. Furthermore, CH$_3$OH can be released from grains in shocks, and thus CH$_3$OH is an outflow tracer expected to be observed in

---

[9] The 285 $M_\odot$ virial mass reported by Cesaroni et al. (1994a) is smaller than our estimate because of the narrower NH$_3$ line width.

[10] Based on 1.4 mm observations, Gibb et al. (2004) report a mass between 156 and 850 $M_\odot$.

TABLE 1
CH₃OH Line Parameters

ID	α (J2000.0)	δ (J2000.0)	S_ν (mJy)	V_{LSR} (km s^{-1})	$\Delta V_{>3\sigma}$[a] (km s^{-1})	$\int S_\nu \, dv$ (mJy km s^{-1})	Notes[b]
1	18 47 33.96	−01 12 48.5	23(4)	99.5(1.3)	6.6(2.6)	77(7)	V
2	18 47 34.02	−01 12 48.3	108(4)	95.5(1.3)	9.3(2.6)	407(8)	V, M
3	18 47 34.15	−01 12 50.0	34(5)	92.9(1.3)	8.0(2.6)	44(8)	V
4	18 47 34.20	−01 12 49.8	419(3)	94.2(1.3)	6.6(2.6)	1265(8)	V
5	18 47 34.26	−01 12 48.9	44(4)	95.5(1.3)	8.0(2.6)	133(8)	V
HMC	18 47 34.31	−01 12 45.9	782(13)	98.05(0.06)	18.5(2.6)	6600(104)	G
6	18 47 34.35	−01 12 48.4	244(6)	102.2(1.3)	15.9(2.6)	906(11)	V, M
7	18 47 34.38	−01 12 47.6	50(9)	100.9(1.3)	10.6(2.6)	248(11)	V, M
8	18 47 34.41	−01 12 46.2	70(6)	102.2(1.3)	12.0(2.6)	165(10)	V, M
9	18 47 34.42	−01 12 40.5	32(4)	100.9(1.3)	6.6(2.6)	84(8)	V
10	18 47 34.46	−01 12 47.8	96(5)	100.9(1.3)	6.6(2.6)	284(8)	V
11	18 47 34.50	−01 12 44.4	55(4)	99.5(1.3)	6.6(2.6)	178(8)	V
12	18 47 34.53	−01 12 46.1	22(4)	95.5(1.3)	9.3(2.6)	52(8)	V, M
13	18 47 34.53	−01 12 43.2	52(4)	102.2(1.3)	9.3(2.6)	127(9)	V, M
14	18 47 34.55	−01 12 43.0	78(7)	98.2(1.3)	8.0(2.6)	87(8)	V, M
15a	18 47 34.59	−01 12 49.0	381(4)	99.5(1.3)	23.9(2.6)	1763(13)	V, M
15b	18 47 34.55	−01 12 48.8	34(4)	86.2(1.3)	18.6(2.6)	1212(12)	V, M

Note.—Units of right ascension are hours, minutes, and seconds, and units of declination are degrees, arcminutes, and arcseconds.

[a] $\Delta V_{>3\sigma}$ is the line width for $S_\nu > 3\sigma$; two channel widths are reported as uncertainty.

[b] G stands for line parameters derived from a Gaussian fit of the line profile shown in Fig. 2, top panel. This is the only spectral feature considered to be thermal. The FWHM of the Gaussian profile is 7.9(0.2) km s^{-1}. The 1 σ statistical noise from the baseline is reported as uncertainty in the peak flux density. Except for the $\Delta V_{>3\sigma}$ uncertainty, the uncertainties are 1 σ errors from the fit. The position corresponds to the centroid of the HMC. The flux density of the peak channel is 817 mJy. V stands for the CH₃OH masers, for which we report the peak position and flux density (and respective errors) obtained with the task JMFIT in AIPS. V_{LSR} is the LSR velocity of the peak intensity channel. We report one channel width as error of V_{LSR} and 2 σ times the square root of the number of channels in the line as error in $\int S_\nu \, dv$. M indicates that multiple maser components overlapped.
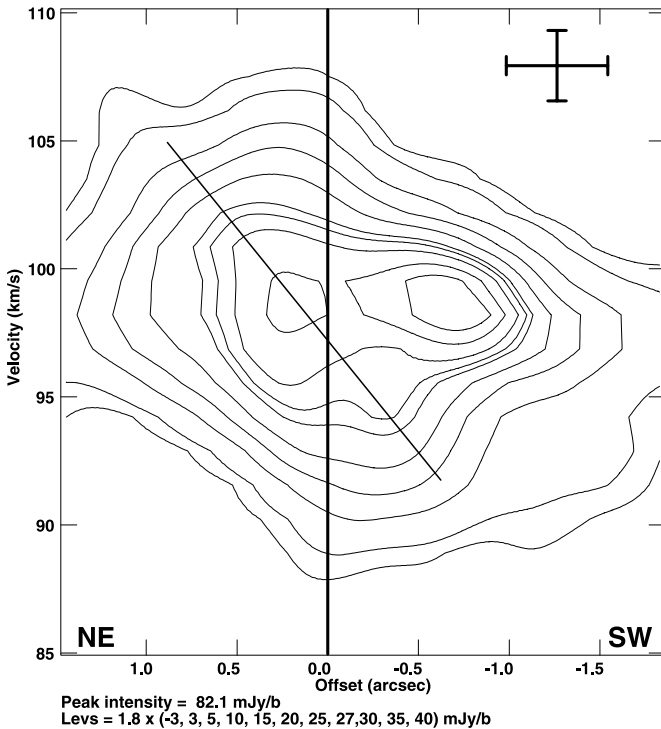
Fig. 3.—Position-velocity diagram along the major axis of the HMC (from the natural weighted data cube; Fig. 1). The cross in the top right corner of the figure represents the error bars for the velocity (two channel widths) and position (θ_{syn}). The thick vertical line marks the location of the geometrical center of a segment connecting the two 7 mm radio continuum sources (see Fig. 1, *bottom panel*). Note the velocity distribution around the center of the HMC (inclined line based on visual inspection) that is consistent with a molecular outflow.

thermal emission toward high-density regions ($\gtrsim 10^7$ cm^{-3}; Mehringer & Menten 1997).

5. CH₃OH OUTFLOW INTERPRETATION WITH RESPECT TO OTHER MOLECULAR TRACERS

In this section we explore the consistency of our outflow interpretation with respect to other molecular tracers:

5.1. *Masers*

In Figure 5 we show with crosses the H₂O (22 GHz) masers detected by Hofner & Churchwell (1996, angular resolution $\sim 0.4''$). The H₂O masers are mostly distributed in northeast-southwest direction, and are coincident with the center of the HMC. Their spatial distribution is similar to the orientation of the CH₃OH velocity gradient reported in this work. H₂O masers are known tracers of shocked gas mostly associated with jets and outflows (e.g., Goddi et al. 2005; Moscadelli et al. 2005; Hofner et al. 2007; see also review by Fish 2008),[11] which supports our interpretation of a CH₃OH outflow in the northeast-southwest direction.

In Figure 5 we also show the distribution of OH 1.667 and 1.665 GHz (*circles*) masers in the region from the Gaume & Mutel (1987) survey. The OH masers are mostly located within the "outflow" region as extrapolated from the CH₃OH bipolar structure. The 1.667 GHz OH masers show a velocity gradient red/blueshifted in the east-west direction, with a slight northeast-southwest inclination and a distribution reminiscent of a precessing jet. Some OH masers have been found associated with bipolar outflows in massive star-forming regions (e.g., Argon et al. 2003; de Buizer 2006). Thus, as in the case of H₂O, the OH maser distribution is consistent with our interpretation of a molecular

[11] H₂O masers have also been claimed to trace disks (e.g., Torrelles et al. 1998).

Grey Scale = [14.4,86.6] mJy/b
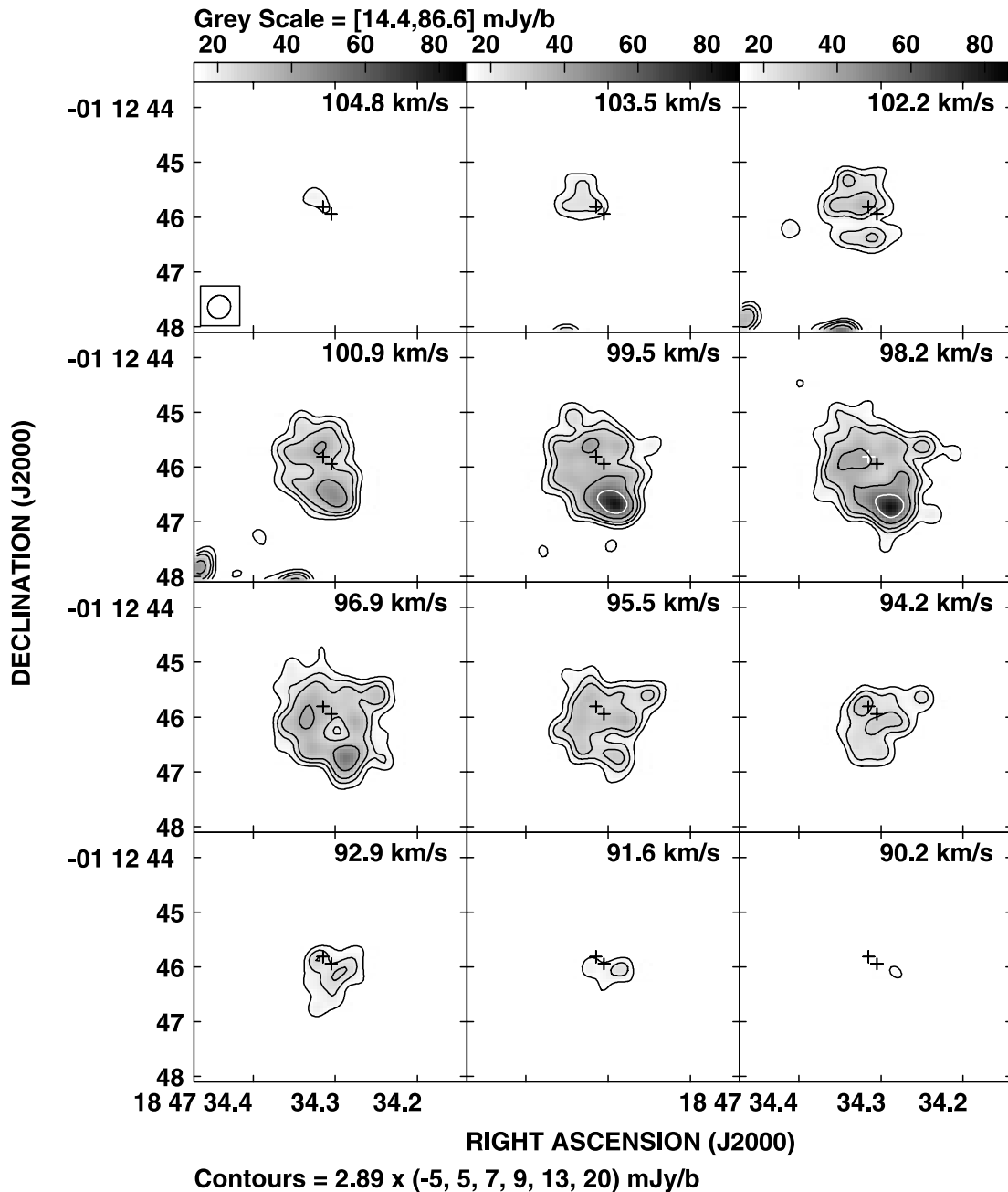
FIG. 4.—Channel maps from the uniform weighted CH$_3$OH cube. The plus signs mark the position of the two 7 mm radio continuum sources shown in Figs. 1 and 5. (Araya et al. 2003; P. Hofner et al. in preparation). Note the CH$_3$OH bipolar lobe morphology from the 92.9 and 103.5 km s^{-1} channels suggestive of a wide-angle outflow oriented at the same position angle as the two 7 mm radio continuum sources.

outflow in the northeast-southwest direction. We note, however, that OH masers also appear to trace torus or disk structures toward other massive star-forming regions (e.g., Edris et al. 2005); thus OH masers are not exclusive tracers of outflow material.

5.2. Nonmaser Outflow Tracers

Olmi et al. (1996) conducted PdBI observations of the ^{13}CO (1–0) line in G31.41+0.31 with a synthesized beam of $\sim 3''$, i.e., substantially lower angular resolution than our observations ($\theta_{syn} \sim 0.4''$). They report two ^{13}CO main spectral components, one at a velocity of ~ 94 km s^{-1}, and the other at ~ 101 km s^{-1}, that are similar to the velocities of the red and blue CH$_3$OH channel maps shown in Figure 5. The ^{13}CO emission is clearly redshifted toward the north and blueshifted toward the south.

Whether the velocity gradient is oriented northwest-southeast or northeast-southwest is a point of controversy: Olmi et al. (1996) argue that the velocity gradient (i.e., the ^{13}CO outflow) is oriented northwest-southeast; however, their conclusion is affected by the presence of multiple clumps in the field, extended ^{13}CO emission, optical depth effects and sparse u-v coverage. Thus, we consider that the precise orientation of the outflow cannot be determined based only on the ^{13}CO data of Olmi et al. (1996); we conclude that the available ^{13}CO data do not invalidate our interpretation of a northeast-southwest outflow.

Other molecular probes that are good tracers of shocked gas in outflows are SiO and H$_2$S (see review by Arce et al. 2007). Gibb et al. (2004) conducted H$_2$S BIMA observations ($\theta_{syn} \sim 1.8''$) and found a velocity gradient dominant in the line core in the
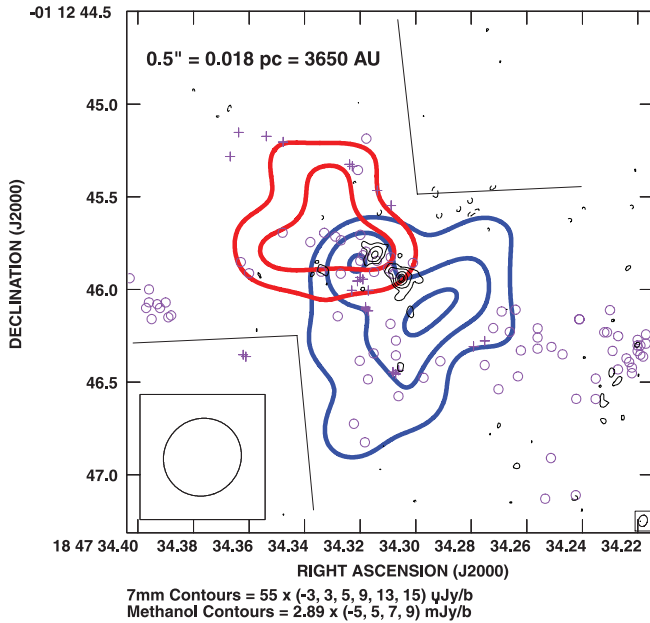
FIG. 5.—In red and blue we show the 92.9 and 103.5 km s^{-1} channel maps from Fig. 4, respectively; in black contours we show the 7 mm continuum from Araya et al. (2003; P. Hofner et al. in preparation). We mark the H$_2$O 22 GHz masers (Hofner & Churchwell 1996) with plus signs (+) and OH masers (Gaume & Mutel 1987) with circles. Note that most of the masers are contained within the extrapolated outflow region (*black lines*).

northeast-southwest direction, while the line wings separate in the east-west direction. They argue that the outflow is in the east-west direction and that the northeast-southwest velocity gradient may instead be tracing rotation of the molecular core. However, after close inspection of Figure 8 and the PV diagrams presented in Gibb et al. (2004), we find that the northeast-southwest and east-west velocity gradients could be interpreted as signatures of a single wide-angle northeast-southwest outflow. Nevertheless, the velocity field seen in H$_2$S is complex, and it is difficult to uniquely disentangle its kinematic components.

Maxia et al. (2001) report Owens Valley Radio Observatory SiO (2–1) observations toward the G31.41+0.31 HMC with $\theta_{syn} = 5.9'' \times 3.7''$. As in the case of CH$_3$OH (Fig. 1) and H$_2$S, they detected a northeast-southwest velocity gradient. Maxia et al. (2001) favor the torus interpretation of the northeast-southwest velocity gradient but state that the data are not conclusive in this regard. The SiO (2–1) transition can be enhanced in shocked regions; thus it is likely that the SiO is tracing outflow material. We conclude that the Maxia et al. (2001) SiO data are consistent with our interpretation of a northeast-southwest outflow.

5.3. *Hot Molecular Cores Tracers*

The HMC in G31.41+0.31 has been observed in several molecular transitions that are typical tracers of hot and/or dense material, i.e., tracers of hot molecular cores.

Cesaroni et al. (1998) conducted high angular resolution ($\theta_{syn} \sim 0.4''$) VLA observations of the NH$_3$ (4,4) main and satellite transitions. As in the case of our CH$_3$OH observations, the NH$_3$ (4,4) main line traces a northeast-southwest elongated structure with a velocity gradient in the same direction. Cesaroni et al. (1998) report that neither the rotation or outflow interpretation of the northeast-southwest velocity gradient can be ruled out; however, they preferred the rotation hypothesis based on the ^{13}CO

observations of Olmi et al. (1996) discussed above. However, it would not be surprising that NH$_3$ is partially tracing the outflow (e.g., Bachiller et al. 1993; Zhang et al. 2007), and thus, the NH$_3$ (4,4) data are consistent with our outflow interpretation.

CH$_3$CN is another well-known tracer of density and temperature in hot molecular cores. Cesaroni et al. (1994b) conducted CH$_3$CN ($J = 6$–5) observations with PdBI ($\theta_{syn} \sim 2''$). They found a northeast-southwest velocity gradient consistent with the kinematics and position of the CH$_3$OH emission reported in this work. They discussed the possible nature of the velocity gradient (outflow or disk), and concluded that both options are possible, but that in either case, the lifetime of the structure should be short (of the order of 10^3–10^4 yr). In subsequent observations, Olmi et al. (1996) report IRAM 30 m + PdBI observations of the $J = 6$–5 transition of CH$_3$CN. The combined IRAM 30 m + PdBI map of the $K = 0 + K = 1$ CH$_3$CN transitions shows an elongation in the northwest-southeast direction, i.e., perpendicular to the CH$_3$OH velocity gradient. We speculate that this northwest-southeast elongated structure could be tracing a molecular torus perpendicular to the northeast-southwest outflow. More recently, Beltrán et al. (2004) report PdBI observations of the $J = 12$–11 transition of CH$_3$CN ($\theta_{syn} \sim 1''$). As in the previous CH$_3$CN observations, they detected a northeast-southwest velocity gradient. Based on the direction of the ^{13}CO velocity gradient reported in Olmi et al. (1996), they ruled out the outflow possibility to explain the northeast-southwest velocity gradient. As mentioned above, we do not consider that the ^{13}CO data of Olmi et al. (1996) unambiguously establish the outflow direction, so the outflow interpretation of the northeast-southwest velocity gradient cannot be ruled out based only on the Olmi et al. (1996) ^{13}CO data. Finally, although CH$_3$CN traces elongated (torus) structures toward several massive star-forming regions (e.g., Cesaroni et al. 1997), we note that CH$_3$CN can also trace molecular outflows in massive star-forming regions (e.g., Wink et al. 1994); therefore, it is not unreasonable to believe that the CH$_3$CN velocity gradient is tracing the molecular outflow in G31.41+0.31, and thus consistent with our northeast-southwest outflow interpretation.

6. IMPLICATIONS OF THE CH$_3$OH OUTFLOW DETECTION

Our observations confirm the existence of an outflow in the G31.41+0.31 HMC, supporting the mounting evidence for outflows during the HMC phase of massive star formation (e.g., Gibb et al. 2004; Hofner et al. 2001). Given the physical characteristics of the outflow (see § 4), it cannot be driven by a low-mass star but rather requires a massive young stellar object as also concluded by Gibb et al. (2004). The CH$_3$OH outflow shows a wide-angle (>60°) bipolar morphology. We cannot rule out that the wide-angle bipolar structure is caused by the superposition of several molecular outflows (e.g., Puga et al. 2006), or whether the outflow is mostly driven by only one young massive (proto)star. If the latter option were correct then our observations would show that young massive (proto)stars can produce wide-angle molecular outflows well before the formation of an UCH II region.

Based on the bipolar wide-angle gas distribution, a circulation model (see Arce et al. 2007) seems as a promising scenario to explain the outflow morphology. If our interpretation of an outflow in the G31.41+0.31 is correct, then infall signatures would be expected. Indeed, Wyrowski et al. (2006) recently reported infall evidence in G31.41+0.31 based on APEX CO observations.

7. SUMMARY

We report high angular resolution VLA observations of CH_3OH emission (44 GHz) toward the massive star-forming region G31.41+0.31. We detected CH_3OH maser emission that is distributed toward the edges of the radio continuum, i.e., at the interface between ionized gas and molecular material, supporting the idea that 44 GHz CH_3OH masers originate in shocked gas environments. The CH_3OH masers are primarily blueshifted toward the southwest of the region, whereas the redshifted masers are mostly toward the east and northeast of the region. We also detected a CH_3OH maser velocity gradient associated with the shell-like UCH II in G31.41+0.31.

We detected CH_3OH (quasi)thermal emission from the G31.41+0.31 HMC symmetrically distributed with respect to the two 7 mm radio continuum sources reported by Araya et al. (2003; P. Hofner et al., in preparation). We found a northeast-southwest velocity gradient in the CH_3OH thermal brightness distribution. We present evidence based on our observations and comparison with other continuum and molecular data that lead us to conclude that the northeast-southwest velocity gradient is likely tracing an outflow. The outflow has a mechanical luminosity of the order of $\sim 20\,L_\odot$, a mass $\gtrsim 15\,M_\odot$, and shows a clear bipolar morphology, supporting the mounting observational evidence for the existence of bipolar massive outflows during the HMC phase. The outflow has a wide opening angle indicating that young massive stellar objects can drive wide-angle flows well before the formation of an observable UCH II region.

REFERENCES

Araya, E., Hofner, P., Kurtz, S., Bronfman, L., & DeDeo, S. 2005, ApJS, 157, 279
Araya, E., Hofner, P., Olmi, L., Linz, H., Kurtz, S., & Cesaroni, R. 2003, in IAU Symp. 221, Star Formation at High Angular Resolution, ed. M. Burton, R. Jayawardhana, & T. Bourke (Cambridge: Cambridge Univ. Press), 489
Arce, H. G., Shepherd, D., Gueth, F., Lee, C.-F., Bachiller, R., Rosen, A., & Beuther, H. 2007, in Protostars & Planets V, ed. B. Reipurth, D. Jewitt, & K. Keil (Tucson: Univ. Arizona Press), 245
Arce, H. G., & Sargent, A. I. 2004, ApJ, 612, 342
Argon, A. L., Reid, M. J., & Menten, K. M. 2003, ApJ, 593, 925
Bachiller, R., Martín-Pintado, J., & Fuente, A. 1993, ApJ, 417, L45
Beltrán, M. T., Cesaroni, R., Neri, R., Codella, C., Furuya, R. S., Testi, L., & Olmi, L. 2004, ApJ, 601, L187
Bonnell, I. A., & Bate, M. R. 2006, MNRAS, 370, 488
Bonnell, I. A., Bate, M. R., & Zinnecker, H. 1998, MNRAS, 298, 93
Cesaroni, R., Churchwell, E., Hofner, P., Walmsley, C. M., & Kurtz, S. 1994a, A&A, 288, 903
Cesaroni, R., Felli, M., Testi, L., Walmsley, C. M., & Olmi, L. 1997, A&A, 325, 725
Cesaroni, R., Galli, D., Lodato, G., Walmsley, C. M., & Zhang, Q. 2007, in Protostars and Planets V, ed. B. Reipurth, D. Jewitt, & K. Keil (Tucson: Univ. Arizona Press), 197
Cesaroni, R., Hofner, P., Walmsley, C. M., & Churchwell, E. 1998, A&A, 331, 709
Cesaroni, R., Neri, R., Olmi, L., Testi, L., Walmsley, C. M., & Hofner, P. 2005, A&A, 434, 1039
Cesaroni, R., Olmi, L., Walmsley, C. M., Churchwell, E., & Hofner, P. 1994b, ApJ, 435, L137
Churchwell, E. 2002, ARA&A, 40, 27
de Buizer, J. M. 2006, ApJ, 642, L57
Edris, K. A., Fuller, G. A., Cohen, R. J., & Etoka, S. 2005, A&A, 434, 213
Fish, V. L. 2008, in Astrophysical Masers and Their Environments, ed. J. Chapman, & W. A. Baan (Cambridge: Cambridge Univ. Press), in press (arXiv: 0704.0242v1)
Gaume, R. A., & Mutel, R. L. 1987, ApJS, 65, 193
Gibb, A. G., Wyrowski, F., & Mundy, L. G. 2004, ApJ, 616, 301

Goddi, C., Moscadelli, L., Alef, W., Tarchi, A., Brand, J., & Pani, M. 2005, A&A, 432, 161
Hofner, P., Cesaroni, R., Olmi, L., Rodríguez, L. F., Martí, J., & Araya, E. 2007, A&A, 465, 197
Hofner, P., & Churchwell, E. 1996, A&AS, 120, 283
Hofner, P., Wiesemeyer, H., & Henning, Th. 2001, ApJ, 549, 425
Kaufman, M. J., Hollenbach, D. J., & Tielens, A. G. G. M. 1998, ApJ, 497, 276
Keto, E., & Wood, K. 2006, ApJ, 637, 850
Klaassen, P. D., Plume, R., Ouyed, R., von Benda-Beckmann, A. M., & Di Francesco, J. 2006, ApJ, 648, 1079
Kurtz, S., Cesaroni, R., Churchwell, E., Hofner, P., & Walmsley, C. M. 2000, in Protostars & Planets IV, ed. V. Mannings, A. Boss & S. Russell (Tucson: Univ. Arizona Press), 299
Kurtz, S., Hofner, P., & Vargas-Álvarez, C. 2004, ApJS, 155, 149
Maxia, C., Testi, L., Cesaroni, R., & Walmsley, C. M. 2001, A&A, 371, 287
Mehringer, D. M., & Menten, K. M. 1997, ApJ, 474, 346
Moscadelli, L., Cesaroni, R., & Rioja, M. J. 2005, A&A, 438, 889
Olmi, L., Cesaroni, R., Neri, R., & Walmsley, C. M. 1996, A&A, 315, 565
Puga, E., Feldt, M., Alvarez, C., Henning, Th., Apai, D., Le Coarer, E., Chalabaev, A., & Stecklum, B. 2006, ApJ, 641, 373
Sewiło, M., Watson, C., Araya, E., Churchwell, E., Hofner, P., & Kurtz, S. 2004, ApJS, 154, 553
Shepherd, D. S., Watson, A. M., Sargent, A. I., & Churchwell, E. 1998, ApJ, 507, 861
Stahler, S. W., Palla, F., & Ho, P. T. P. 2000, in Protostars & Planets IV, ed. V. Mannings, A. Boss & S. Russell (Tucson: Univ. Arizona Press), 327
Torrelles, J. M., Gómez, J. F., Rodríguez, L. F., Curiel, S., Anglada, G., & Ho, P. T. P. 1998, ApJ, 505, 756
Wink, J. E., Duvert, G., Guilloteau, S., Güsten, R., Walmsley, C. M., & Wilson, T. L. 1994, A&A, 281, 505
Wyrowski, F., Heyminck, S., Güsten, R., & Menten, K. M. 2006, A&A, 454, L95
Yorke, H. W., Bodenheimer, P., & Laughlin, G. 1995, ApJ, 443, 199
Zhang, Q., Sridharan, T. K., Hunter, T. R., Chen, Y., Beuther, H., & Wyrowski, F. 2007, A&A, 470, 269